Search for an Ultralight Scalar Dark Matter Candidate with the AURIGA Detector

Antonio Branca,[1] Michele Bonaldi,[2,3] Massimo Cerdonio,[1] Livia Conti,[1] Paolo Falferi,[3,4] Francesco Marin,[5,6,7] Renato Mezzena,[3,8] Antonello Ortolan,[9] Giovanni A. Prodi,[3,8] Luca Taffarello,[1] Gabriele Vedovato,[1] Andrea Vinante,[4] Stefano Vitale,[3,8] and Jean-Pierre Zendri[1]

[1]*INFN, Sezione di Padova, Via Marzolo 8, I-35131 Padova, Italy*
[2]*Institute of Materials for Electronics and Magnetism, Nanoscience-Trento-FBK Division, I-38123 Trento, Italy*
[3]*TIFPA—INFN, c/o Dipartimento di Fisica, Universitá di Trento, Via Sommarive 14, 38123 Povo, Trento, Italy*
[4]*Istituto di Fotonica e Nanotecnologie, CNR—Fondazione Bruno Kessler, I-38123 Povo, Trento, Italy*
[5]*Dipartimento di Fisica e Astronomia, Universitá di Firenze, Via Sansone 1, I-50019 Sesto Fiorentino (FI), Italy*
[6]*Istituto Nazionale di Fisica Nucleare (INFN), Sezione di Firenze, Via Sansone 1, I-50019 Sesto Fiorentino (FI), Italy*
[7]*European Laboratory for Non-Linear Spectroscopy (LENS), Via Carrara 1, I-50019 Sesto Fiorentino (FI), Italy*
[8]*Dipartimento di Fisica, Universitá di Trento, I-38123 Povo, Trento, Italy*
[9]*INFN—Laboratori Nazionali di Legnaro, I-35020 Legnaro (PD), Italy*

(Received 28 July 2016; published 12 January 2017)

A search for a new scalar field, called moduli, has been performed using the cryogenic resonant-mass AURIGA detector. Predicted by string theory, moduli may provide a significant contribution to the dark matter (DM) component of our Universe. If this is the case, the interaction of ordinary matter with the local DM moduli, forming the Galaxy halo, will cause an oscillation of solid bodies with a frequency corresponding to the mass of moduli. In the sensitive band of AURIGA, some 100 Hz at around 1 kHz, the expected signal, with $Q = \triangle f/f \sim 10^6$, is a narrow peak, $\triangle f \sim 1$ mHz. Here the detector strain sensitivity is $h_s \sim 2 \times 10^{-21}$ Hz$^{-1/2}$, within a factor of 2. These numbers translate to upper limits at 95% C.L. on the moduli coupling to ordinary matter $(d_e + d_{m_e}) \lesssim 10^{-5}$ around masses $m_\phi = 3.6 \times 10^{-12}$ eV, for the standard DM halo model with $\rho_{\mathrm{DM}} = 0.3$ GeV/cm^3.

DOI: 10.1103/PhysRevLett.118.021302

Introduction.—A possible source of dark matter (DM) is an ultralight scalar field, Φ, with couplings to standard model (ordinary) matter weaker than the gravitational strength [1,2]. For instance, this field may be the moduli field, which is predicted by string theory. The coupling of this light field with ordinary matter implies a dependence of the constants of nature on Φ [1]. In particular, electron mass, m_e, and fine structure constant, α, vary with respect to their nominal values following

$$m_e(\mathbf{x}, t) = m_{e,0}[1 + d_{m_e}\sqrt{4\pi G_N}\Phi(\mathbf{x}, t)] \quad (1)$$

$$\alpha(\mathbf{x}, t) = \alpha_0[1 + d_e\sqrt{4\pi G_N}\Phi(\mathbf{x}, t)] \quad (2)$$

where G_N is the Newton's constant and d_{m_e} (d_e) is the dimensionless coupling of moduli to electrons (photons): Φ can be identified with an electron mass modulus if $d_{m_e} \neq 0$ or an electromagnetic gauge modulus if $d_e \neq 0$. Given relations (1) and (2), if the field Φ makes up a significant fraction of the local DM density, the volume of a solid will oscillate in time [1]. In fact, assuming the mass of these particles, m_Φ, to be small enough compared to the energy density of the DM, their number density within our Galaxy is high and the field Φ can be described as a classical wave, instead of individual particles:

$$\Phi(\mathbf{x}, t) = \Phi_0 \cos[m_\Phi(t - \mathbf{v}\cdot\mathbf{x})] + O(v^2), \quad (3)$$

where $|\mathbf{v}|$ is the relative velocity of DM with respect to Earth, roughly equal to the virial velocity in our Galaxy. Thus, the interaction of ordinary matter with the surrounding DM field would make m_e and α oscillate in time, causing a fluctuation of the atoms size, $r_0 \sim 1/\alpha m_e$, in a solid. This would imply a variation $\triangle L$ of the length of a body, corresponding to a relative deformation with respect to its equilibrium length, L_0, given by

$$h(t) = \frac{\triangle L(t)}{L_0} = \frac{\sqrt{4\pi}}{M_{\mathrm{Pl}}}(d_{m_e} + d_e)\Phi(t), \quad (4)$$

where M_{Pl} is the Planck mass and $\Phi(t)$ the moduli field. To calculate the power spectrum of relative deformation h, we use the so-called standard halo model (SHM) that assumes a spherical DM halo for the Galaxy with local DM density $\rho_{\mathrm{DM}} = 0.3$ GeV/cm^3, and an isotropic Maxwell-Boltzmann speed distribution [3]. In this framework, if moduli account for a significant fraction of DM in our Universe then the corresponding field $\Phi(t)$ can be described as a zero mean stochastic process with a Maxwell-Boltzmann power spectrum density [4], consequently the spectrum of the relative deformation h is given by

$$h(f) = h_0 \frac{(d_{m_e} + d_e)}{a^{\frac{3}{4}} f_\phi}(|f| - f_\phi)^{\frac{1}{4}} e^{-(|f|-f_\phi)/2a}\Theta(|f| - f_\phi) \quad (5)$$

where $h_0 = 1.5 \times 10^{-16}$ Hz is a constant, $f_\phi = m_\Phi/2\pi$ is the frequency corresponding to moduli with a given mass, $a = 1/3 f_\phi \langle v^2 \rangle$ and $\langle v^2 \rangle / c^2 \sim 10^{-6}$ the mean squared velocity of the DM halo. Equation (5) tells us that the signal strain is a monopole (isotropic strain) and approximately monochromatic.

In this work, we analyze the data of the resonant-mass gravitational wave detector AURIGA [5], searching for the strain induced by hypothetical moduli DM, expressed by Eq. (5). AURIGA represents the state of the art in the class of gravitational wave cryogenic resonant-mass detectors. It is located at the INFN National Laboratory of Legnaro (Italy) and has been in continuous operation since the year 2004. The detector is based on a 2.2×10^3 kg, 3 m long bar made of low-loss aluminum alloy (Al5056), cooled to liquid helium temperatures. The fundamental longitudinal mode of the bar, sensitive to the moduli induced oscillation, has an effective mass $M = 1.1 \times 10^3$ kg and a resonance frequency $\omega_B/2\pi \simeq 900$ Hz. Figure 1 shows a scheme of the detector core and readout: the bar resonator is coupled to the fundamental flexural mode of a mushroom-shaped lighter resonator, with 6 kg effective mass and the same resonance frequency. As the mechanical energy is transferred from the bar to the lighter resonator, the motion is magnified by a factor of roughly 15. A capacitive transducer [6], biased with a static electric field of 10^7 V/m, converts the differential motion between the bar and mushroom resonator into an electrical current, which is finally detected by a low noise dc SQUID amplifier [7] through a low-loss high-ratio superconducting transformer [8]. The transducer efficiency is further increased by placing the resonance frequency of the electrical LC circuit close to the mechanical resonance frequencies [6], at 930 Hz. The detector can then be simply modeled as a system of three coupled resonators: its dynamics is described by three normal modes at separate frequencies, each one being a superposition of the bar and transducer mechanical resonators and the LC electrical resonator [9]. The bar resonator motion is detected with a

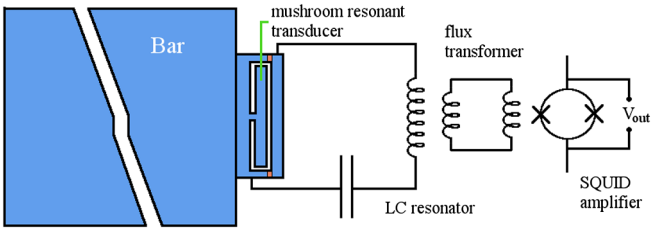

FIG. 1. Scheme of the gravitational wave detector AURIGA. The system comprises three coupled resonators with nearly equal resonant frequency of about 900 Hz: the first longitudinal mode of the cylindrical bar, the first flexural mode of the mushroom-shaped resonator, which is also one of the plates of the electrostatic capacitive transducer, and the low-loss electrical LC circuit. The electrical current of the LC resonator is detected by a low noise dc SQUID amplifier.

sensitivity of order several 10^{-21} m Hz$^{-1/2}$ over a ~100 Hz bandwidth. The spectral noise floor in the relative deformation for the fundamental longitudinal mode, for the frequency interval of maximum sensitivity is given in Fig. 2. This sensitivity is accomplished thanks to the multimode resonant capacitive transducer combined with the very low noise dc SQUID amplifier.

Analysis workflow and data set.—Output from the readout chain of the AURIGA detector is digitized with a sampling frequency of $f_s = 4882.8$ Hz through an Analog to Digital Converter. As stated above, the motion of the bar from the equilibrium length is converted into an electrical signal. A calibration function obtained by a thorough mechanical characterization of the system [9] is then used to convert data from the electrical potential difference to the relative deformation h of the AURIGA bar length. Equation (5) shows that the relative deformation induced by signal moduli, would be a sharp resonance around the frequency corresponding to the moduli mass. Therefore, a possible signal could be spotted by analyzing the noise power spectrum of the calibrated AURIGA output $P_{\rm cal}(f)$. $P_{\rm cal}(f)$ gives the information concerning the relative deformation of the bar:

$$h^2 = \int_{\triangle f} P_{\rm cal}(f) df. \tag{6}$$

The expected signal [Eq. (5)] has a bandwidth of about $\triangle f \sim 1$ mHz in the sensitive band of AURIGA. Therefore,

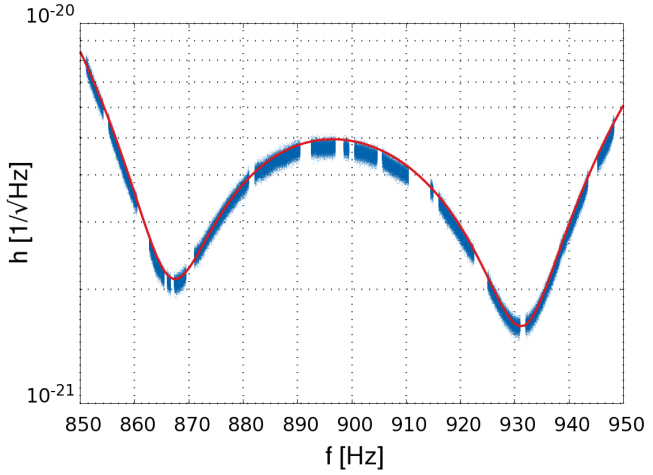

FIG. 2. Frequency spectrum of the bar relative deformation computed on August 2015 AURIGA data (blue curve), obtained by averaging $N = 400$ power spectrums from one-hour-long data streams. The experimental result is compared to the predicted noise power spectrum density by Fluctuation-Dissipation theorem (red line), showing a good matching. The thickness of the data curve is due to the noise variance, reduced by averaging the power spectrums. Holes in data correspond to excluded spurious peaks associated with the known external background. Moreover, these spurious peaks have shape and width not matching the expectation from the moduli signal [see Fig. 3].

we split the analyzed data set into one-hour-long data streams and perform power spectrum computation on each stream to achieve the proper spectrum resolution. Computed power spectrums are averaged to reduce the noise standard deviation and achieve a better sensitivity. If N is the number of averaged power spectrums, the variance of the noise is $N^{1/2}$ [10], and the corresponding standard deviation on h decreases with the number of averages as $N^{1/4}$. Thus, a good sensitivity on the moduli signal is already achieved with few weeks of data. Using the entire data set acquired by AURIGA (∼10 years) would improve the sensitivity just by a factor of 3. The search for the DM moduli is then performed on a data set one month long (acquired by the AURIGA detector during August 2015). The AURIGA detector was running under stable conditions; stability of the detector is inferred by the stable frequencies and shape of the three main detector's modes, checked by studying the evolution of the detector power spectrum on the analyzed data set. Spikes in time due to energetic background events could hide a possible signal from moduli and must be removed from the data set: for each data stream in the time domain the rms is computed, obtaining a distribution of the rms value for the whole data set; data affected by energetic background lie in the high value tail of the distribution. A cut on the rms is then set to discard data with large rms values. This cut still allows us to maintain a 86% duty cycle of the detector.

After cleaning data streams with a rms cut, they are windowed in the time domain using a Hann window type, which allows a good frequency resolution and reduced spectral leakage. The measured bar relative deformation spectrum is shown in Fig. 2. As shown by the figure, the measured noise is in excellent agreement with the predicted noise behavior. The latter has been obtained out of the sum of computed contributions from each noise source, in turn derived by measured experimental parameters [9]. Few spurious peaks, known to be associated with external background sources, have been excluded from the analysis.

Simulation.—To prove we are able to detect this signal with AURIGA, a simulation has been performed to study the actual signal bandwidth within the detector sensitive region and to fine-tune the analysis workflow. Equation (5) is exploited to simulate a signal with $f_\phi \backsimeq 867$ Hz and coupling $(d_e + d_{m_e}) = 5 \times 10^{-4}$, which is smaller than the natural values expected for d_{m_e} [1]. f_ϕ lies close to the first minimum of the AURIGA noise curve, shown in Fig. 2. Given the narrow bandwidth of this signal, we assumed the noise to be white, $\langle n_i \rangle = 0$, $\langle n_i n_j \rangle = \sigma^2 \delta_{ij}$, around the signal peak, with a standard deviation $\sigma = 2 \times 10^{-21}$ $\mathrm{Hz}^{-1/2}$, equal to the noise level at $f_\phi \backsimeq 867$ Hz (see Fig. 2). We have generated an amount of data comparable to the real data set and applied our analysis pipeline obtaining the result shown in Fig. 3. The spectrum of the simulated signal is spread around ∼10 bins of the spectrum as shown in Fig. 3, blue triangles. The simulated data have been injected into the real data set and in Fig. 3, red circles, we show that the injected signal is well reconstructed at the frequency f_ϕ and it is not removed by the rms cut applied to the data streams. We also show the theoretical signal plus noise, Fig. 3, green line, obtained using same parameters as for the simulation. The little discrepancy between theory and simulation (injection), can be attributed to the minimal leakage due to the windowing of data.

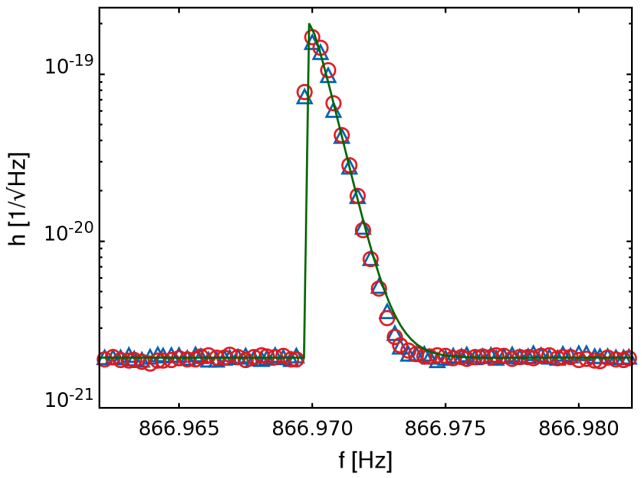

FIG. 3. (blue triangle) Simulation of a moduli signal with moduli couplings $(d_e + d_{m_e}) = 5 \times 10^{-4}$ and frequency $f_\phi \backsimeq 867$ Hz plus white noise with standard deviation $\sigma = 2 \times 10^{-21}$ $\mathrm{Hz}^{-1/2}$, equal to the detector noise level at f_ϕ. (red circle) Same simulated signal injected into the real data. The signal is a narrow peak with a $\triangle f \backsimeq 1$ mHz bandwidth and spread around about 10 bins. (green line) Plot of the power density spectrum in Eq. (5) plus a constant accounting for the white noise with the same parameters of the simulation.

Statistical analysis.—The procedure followed for the statistical analysis of the result shown in Fig. 2 is the one proposed by Feldman and Cousin [11]. Each bin of the distribution in Fig. 2 has a contribution from the noise and a possible contribution from the signal. The squared value of a bin is the result of averaging N power spectrums, then its distribution follows a noncentral χ^2 with N degree of freedom. Since in our case $N \sim 400$ the squared bin distribution can be approximated by the following Gaussian:

$$P(\bar{x}|\mu) = C \exp\left(-\frac{(\bar{x} - \sigma^2 - \mu^2)^2}{\frac{2}{N}\sigma^4(1 + 2\frac{\mu^2}{\sigma^2})}\right) \tag{7}$$

with normalization factor

$$C = \frac{N^{1/2}}{\sigma^2\sqrt{2\pi(1 + 2\frac{\mu^2}{\sigma^2})}} \tag{8}$$

where $\bar{x}$ is the squared bin content, σ^2 is the expected noise level and μ the signal strength. The statistical behavior of the bins in the distribution of Fig. 2 is confirmed by data as predicted by Eq. (7). This is shown in Fig. 4. By means of

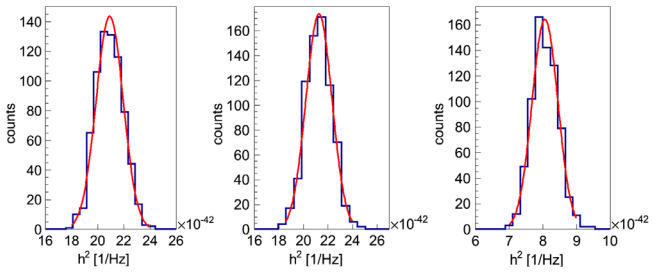

FIG. 4. Distributions of the possible values of three generic bins in the relative bar deformation spectrum shown in Fig. 2. The distributions are well fitted by a Gaussian (red lines) with a mean equal to the noise level at the considered bin frequency and a standard deviation the standard deviation of the noise: (left) $f = 857$ Hz, $\langle h^2 \rangle = 2.1 \times 10^{-41}$ Hz^{-1}, $\sigma_{h^2} = 1.0 \times 10^{-42}$ Hz^{-1}, $\chi^2/ndf = 12.2/8$; (center) $f = 890$ Hz, $\langle h^2 \rangle = 2.1 \times 10^{-41}$ Hz^{-1}, $\sigma_{h^2} = 1.1 \times 10^{-42}$ Hz^{-1}, $\chi^2/ndf = 4.8/5$; (right) $f = 940$ Hz $\langle h^2 \rangle = 8.1 \times 10^{-42}$ Hz^{-1}, $\sigma_{h^2} = 3.8 \times 10^{-43}$ Hz^{-1}, $\chi^2/ndf = 8.3/7$.

Eq. (7) we build the confidence belt in the parameter space $(\bar{x}, \mu^2)$, delimited by the values $(x_1(\mu), x_2(\mu))$ such that

$$\int_{x_1(\mu)}^{x_2(\mu)} P(\bar{x}|\mu) d\bar{x} = P(\mu) \tag{9}$$

for each value of the signal strength μ and a confidence level $P(\mu) = 0.95$. The contributions to the integral in Eq. (9) are ordered following a specific ordering function, as reported in Ref. [11], in order to avoid problems on the parameter estimation near the physical bounds of such parameters. Equation (9) states that for a fixed hypothetical signal strength μ, the observed value of the bin content $\bar{x}$ falls within the interval $(x_1(\mu), x_2(\mu))$ with a probability equal to $P(\mu)$. Thus, for each measured value of $\bar{x}$ the upper and lower limits on the measured signal strength, containing the true value μ with a 95% probability, are obtained by inversion of the constructed confidence belt. We set a threshold, $\bar{x}_{\rm th}$, corresponding to a maximum false alarm probability of finding a signal, which is not actually there, equal to 3 standard deviations away from the background only hypothesis. For observed values of $\bar{x}$ below $\bar{x}_{\rm th}$ we set an upper limit on the signal strain. Values above the threshold $\bar{x}_{\rm th}$ would correspond to an observed signal. Since in our measurement in Fig. 2 we do not observe values exceeding the threshold, we set upper limits on h at 95% confidence level. Interpreting these upper limits as given by moduli through Eq. (5), we convert these values in upper limits on the sum of the couplings of an electromagnetic gauge modulus and an electron mass modulus $(d_e + d_{m_e})$ to ordinary matter. To improve the upper limits, we exploited the noise curve obtained adding the thermal noise prediction from Fluctuation-Dissipation theorem and the noise contribution from the SQUID. By performing a least squares fit of data in Fig. 2, we obtained the upper limits at 95% C.L. from the χ^2 distribution. This allows us to get better upper limits by taking into account a more precise estimation of errors from the fit. Further improvement is obtained by averaging bins in groups of 10 for data in Fig. 2, since the signal would be distributed around ~10 bins, as shown by Fig. 3.

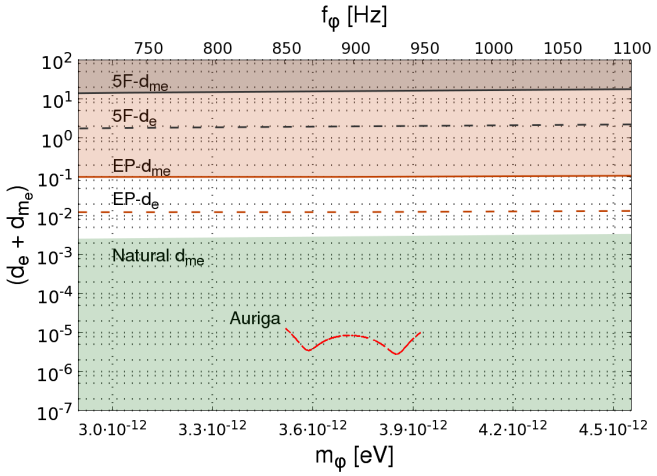

FIG. 5. Upper limits on the sum of the moduli couplings $(d_e + d_{m_e})$ to ordinary matter (red curve) obtained from AURIGA data and reported in the moduli parameter space: bottom and top horizontal axes represent the moduli mass m_ϕ and corresponding frequency $f_\phi = m_\phi/2\pi$, vertical axis represents the sum of moduli coupling $(d_e + d_{m_e})$ values. Depicted green area shows the natural parameter space preferred by theory. Other regions represent 95% C. L. limits on fifth-force tests (5F, gray) and equivalence-principle tests (EP, orange): continuous curves (5F-d_{m_e} and EP-d_{m_e}) refer to upper limits on d_{m_e}, whereas dashed curves (5F-d_e and EP-d_e) refer to upper limits on d_e.

Results.—Final upper limits are reported in Fig. 5. The upper limits set on the sum of the moduli couplings to ordinary matter are better then $(d_e + d_{m_e}) \simeq 10^{-5}$ in the sensitive band of AURIGA, $\triangle f = [850, 950]$ Hz, and explore an interesting physical region of the parameter space, within the natural parameter space for moduli [1]. The same figure reports upper limits on moduli couplings obtained, as discussed in Ref. [1], from fifth-force (5F) [12] and equivalence principle (EP) [13] tests. These are sensitive to different linear combinations of the moduli couplings, d_e and d_{m_e}; therefore, they are able to set limits on the individual couplings. As shown by Fig. 5, these limits are not probing the interesting parameter space in the region where AURIGA is sensitive. With this result we prove that AURIGA, a gravitational wave resonant detector, would be capable of detecting light DM candidates with an interesting sensitivity within its bandwidth. We point out that this level of sensitivity can be achieved only by resonant mass detectors, and not by modern laser interferometers developed for gravitational wave detection, such as LIGO [14] and Virgo [15], even if these have better sensitivity than resonant mass detectors for gravitational waves and recently observed the first event due to a gravitational wave signal [16]. In fact, because of the monopole nature of the expected moduli strain, we do not

expect an interference signal as output from the interferometer due to moduli. Instead, since ultralight scalars can mediate Yukawa forces between objects, one can explore which is the expected effect on the relative position between mirrors within an interferometer arm. This would not be as efficient as exploiting the quadrupole gravitational wave effect on interferometers [17].

M. C. is very grateful to Asimina Arvanitaki for calling attention to the matter and for initial discussions. A. B., M. C., A. O., and L. T. thank Asimina Arvanitaki and Ken Van Tilburg for enlightening discussions and for a critical reading of the manuscript. This work is funded by Istituto Nazionale di Fisica Nucleare.

[1] A. Arvanitaki, S. Dimopoulos, and K. V. Tilburg, Sound of Dark Matter: Searching for Light Scalars with Resonant-Mass Detectors, Phys. Rev. Lett. **116**, 031102 (2016).

[2] A. Khmelnitsky and V. Rubakov, Pulsar timing signal from ultralight scalar dark matter, J. Cosmol. Astropart. Phys. 02 (2014) 019.

[3] J. D. Lewin and P. F. Smith, Review of mathematics, numerical factors, and corrections for dark matter experiments based on elastic nuclear recoil, Astropart. Phys. 6 (**1996**) 87.

[4] L. Krauss, J. Moody, F. Wilczek, and D. E. Morris, Calculations for Cosmic Axion Detection, Phys. Rev. Lett. **55**, 1797 (1985).

[5] M. Cerdonio *et al.*, The ultracryogenic gravitational-wave detector AURIGA, Classical Quantum Gravity **14**, 1491 (1997).

[6] L. Baggio *et al.*, 3-Mode Detection for Widening the Bandwidth of Resonant Gravitational Wave Detectors, Phys. Rev. Lett. **94**, 241101 (2005).

[7] A. Vinante, R. Mezzena, G. Andrea Prodi, S. Vitale, M. Cerdonio, P. Falferi, and M. Bonaldi, Dc superconducting quantum interference device amplifier for gravitational wave detectors with a true noise temperature of 16 μK, Appl. Phys. Lett. **79**, 2597 (2001).

[8] M. Bonaldi, P. Falferi, R. Dolesi, M. Cerdonio, and S. Vitale, High Q tunable *LC* resonator operating at cryogenic temperature, Rev. Sci. Instrum. **69**, 3690 (1998).

[9] A. Vinante, Present performance and future upgrades of the AURIGA capacitive readout, Classical Quantum Gravity **23**, S103 (2006).

[10] D. G. Manolakis and J. G. Proakis, *Digital Signal Processing: Principles, Algorithms and Applications* (Prentice-Hall, Upper Saddle River, NJ, 1996), 3rd ed., Chap. 12, p. 908.

[11] G. J. Feldman and R. D. Cousin, A Unified approach to the classical statistical analysis of small signals, Phys. Rev. D **57**, 3873 (1998).

[12] E. Adelberger, B. R. Heckel, and A. Nelson, Tests of the gravitational inverse-square law, Annu. Rev. Nucl. Part. Sci. **53**, 77 (2003).

[13] S. Schlamminger, K.-Y. Choi, T. A. Wagner, J. H. Gundlach, and E. G. Adelberger, Test of the Equivalence Principle Using a Rotating Torsion Balance, Phys. Rev. Lett. **100**, 041101 (2008).

[14] LIGO Scientific Collaboration, Advanced LIGO, Classical Quantum Gravity **32**, 074001 (2015).

[15] Virgo Collaboration, Advanced Virgo: A second-generation interferometric gravitational wave detector, Classical Quantum Gravity **32**, 024001 (2014).

[16] LIGO Scientific Collaboration and Virgo Collaboration, Observation of Gravitational Waves from a Binary Black Hole Merger, Phys. Rev. Lett. **116**, 061102 (2016).

[17] A. Arvanitaki, J. Huang, and K. V. Tilburg, Searching for Dilaton Dark Matter with Atomic Clocks, Phys. Rev. D **91**, 015015 (2015).